



## RESEARCH ARTICLE

# The anodic dissolution kinetics of Mg alloys in water based on ab initio molecular dynamics simulations

Jieqiong Yan<sup>1</sup> | Xinchun Xu<sup>2</sup> | Gaoning Shi<sup>1</sup> | Yaowei Wang<sup>3</sup> | Chaohong Guan<sup>1</sup> |  
Yuyang Chen<sup>2</sup> | Yao Yang<sup>2</sup>  | Tao Ying<sup>2</sup> | Hong Zhu<sup>1,2</sup>  | Qingli Tang<sup>4</sup> |  
Xiaoqin Zeng<sup>2</sup>

<sup>1</sup>University of Michigan – Shanghai Jiao Tong University Joint Institute, Shanghai Jiao Tong University, Shanghai, China

<sup>2</sup>State Key Laboratory of Metal Matrix Composites, Shanghai Jiao Tong University, Shanghai, China

<sup>3</sup>Shenyang Aircraft Industry Co., Ltd., Technology Research Institute, Shenyang, China

<sup>4</sup>Shanghai Advanced Research Institute, Chinese Academy of Sciences, Shanghai, China

## Correspondence

Hong Zhu and Qingli Tang.

Email: [hong.zhu@sjtu.edu.cn](mailto:hong.zhu@sjtu.edu.cn) and [tangql@sari.ac.cn](mailto:tangql@sari.ac.cn)

## Abstract

The corrosion susceptibility of magnesium (Mg) alloys presents a significant challenge for their broad application. Although there have been extensive experimental and theoretical investigations, the corrosion mechanisms of Mg alloys are still unclear, especially the anodic dissolution process. Here, a thorough theoretical investigation based on ab initio molecular dynamics and metadynamics simulations has been conducted to clarify the underlying corrosion mechanism of Mg anode and propose effective strategies for enhancing corrosion resistance. Through comprehensive analyses of interfacial structures and equilibrium potentials for Mg(0001)/H<sub>2</sub>O interface models with different water thicknesses, the Mg(0001)/72 H<sub>2</sub>O model is identified to be reasonable with −2.17 V vs. standard hydrogen electrode equilibrium potential. In addition, utilizing metadynamics, the free energy barrier for Mg dissolution is calculated to be 0.835 eV, enabling the theoretical determination of anodic polarization curves for pure Mg that aligns well with experimental data. Based on the Mg(0001)/72 H<sub>2</sub>O model, we further explore the effects of various alloying elements on anodic corrosion resistance, among which Al and Mn alloying elements are found to enhance corrosion resistance of Mg. This study provides valuable atomic-scale insights into the corrosion mechanism of magnesium alloys, offering theoretical guidance for developing novel corrosion-resistant Mg alloys.

## KEYWORDS

AIMD, corrosion, equilibrium potential, Mg atom dissolution, polarization curve

## 1 | INTRODUCTION

Magnesium (Mg) alloys, renowned for their lightweight properties, find diverse applications in industries such as aerospace, automotive engineering, and biomedical engineering.<sup>[1–5]</sup> However, the inherent susceptibility of Mg alloys to corrosion in aqueous environments has consistently impeded their widespread utilization.<sup>[6–8]</sup> Nowadays, various strategies have been explored to enhance the corrosion

resistance of Mg alloys, including surface modification,<sup>[9,10]</sup> developing a more protective surface coating,<sup>[11–13]</sup> and so on. However, once metallic magnesium is exposed, the occurrence of the corrosion reaction becomes inevitable.<sup>[14]</sup> Therefore, enhancing the intrinsic corrosion resistance of magnesium is the most fundamental approach.

High-purity Mg exhibits better corrosion resistance but is difficult to produce. When Mg coupled to common alloy elements, galvanic corrosion occurs and results in a significantly

This is an open access article under the terms of the Creative Commons Attribution License, which permits use, distribution and reproduction in any medium, provided the original work is properly cited.

© 2024 The Author(s). *Materials Genome Engineering Advances* published by Wiley-VCH GmbH on behalf of University of Science and Technology Beijing.

elevated corrosion rate. Atrons et al.<sup>[5]</sup> hold that the Mg alloys with corrosion rates less than the intrinsic rate of high-purity Mg in concentrated chloride solution, 0.3 mm/y, is stainless. Cao et al.<sup>[15]</sup> reported the corrosion rate of ultra-high-purity Mg was approximately 0.25 mm/y, and our group<sup>[16]</sup> had previously reported the stainless Mg alloy by adding Al alloying elements with the corrosion rate lower than 0.2 mm/y. However, the experimental research studies are dominated by trial-and-error, and the corrosion mechanisms of Mg alloys are still under debate. Therefore, clarifying the corrosion mechanisms is pivotal to guide the design of corrosion-resistant Mg alloys.

Recent experimental studies have also tended to uncover the corrosion mechanisms of Mg alloys, including reactions at the Mg/water interface and the effect of a surface film.<sup>[17–19]</sup> However, due to the rapid onset of corrosion reactions and the subsequent formation of corrosion products, experimental characterization poses challenges in understanding corrosion reactions of Mg at the microscale, and density functional theory (DFT) simulations are attaining more and more attentions from material scientists to investigate the corrosion mechanisms from the atomic scale. The corrosion of Mg can be divided into two parts: the anodic dissolution process and the cathodic hydrogen evolution reaction (HER). Some efforts have been dedicated to hindering the HER.<sup>[20,21]</sup> For example, our prior work on high-throughput computational screening of Mg binary intermetallics<sup>[6]</sup> has identified some promising Mg intermetallic phases with sluggish HER kinetics, aligning well with experimental results. Besides, we contend that addressing the anodic dissolution process is equally pivotal for enhancing the intrinsic corrosion resistance of Mg alloys.

The anode in the corrosion process of multi-phase Mg alloys primarily consists of the Mg solid solution. The anodic reaction involves the dissolution of Mg atoms from the solid solution matrix, expressed as  $\text{Mg} \rightleftharpoons \text{Mg}^{n+} + n\text{e}^-$ . The corrosion rate can be characterized by the polarization curves based on Equation (1) (detailed discussion can be found in Supporting Information S1).

$$I = I_0 \left\{ \exp \left[ \frac{anF(E - E_e)}{RT} \right] - \exp \left[ -\frac{(1 - \alpha)nF(E - E_e)}{RT} \right] \right\} \quad (1)$$

$$I_0 = nFc_A \frac{KT}{h} \exp \left( \frac{-\Delta G_{\text{Mg} \rightarrow \text{Mg}^{n+}} + anF\Phi_e}{RT} \right) \quad (2)$$

where  $I_0$  is the exchange current density,<sup>[22]</sup>  $n$  is the number of electrons that involved in Mg atom dissolution,  $\alpha$  is the transfer coefficient,  $E_e$  is the equilibrium potential,  $\Phi_e$  is the absolute electrode potential,  $\Delta G_{\text{Mg} \rightarrow \text{Mg}^{n+}}$  is the free energy barrier of dissolution reaction and  $F$ ,  $R$ ,  $T$ ,  $K$ ,  $h$ ,  $c_A$  are Faraday constant, gas constant, absolute temperature, Boltzmann constant, Planck constant and the concentration of reductant (or oxidizer for reverse reaction), respectively.

In Equations (1) and (2), only the values of  $\Phi_e$  and  $\Delta G_{\text{Mg} \rightarrow \text{Mg}^{n+}}$  cannot be obtained directly from experiments. By combining the anodic polarization curve with the cathodic polarization curve, it becomes readily apparent how to determine the overall polarization curve as well as the corrosion current density and the corrosion potential.

If one can obtain crucial parameters such as absolute electrode potential  $\Phi_e$ , and free energy barrier of Mg dissolution  $\Delta G_{\text{Mg} \rightarrow \text{Mg}^{n+}}$  from ab initio calculations, the anodic polarization curves can be obtained theoretically. Such works have been performed by several researchers with some approximations. For example, Ma et al.<sup>[23]</sup> investigated the anisotropic anodic dissolution of Mg alloys, elucidating the relationship between electrode potential and current density using the work function and the surface energy. They calculated  $\Delta G_{\text{Mg} \rightarrow \text{Mg}^{n+}}$  as 30% of the total energy needed to break chemical bonds in bulk Mg to form  $\text{Mg}^{2+}$  and determined  $\Phi_e$  for different Mg surfaces from the work function, which were later aligned with the pure Mg equilibrium potential  $-2.37$  V vs. standard hydrogen electrode (SHE). However, the detailed interaction of water and Mg surface has been overlooked in the prior atomic simulations for corrosion, given that Mg corrosion predominantly occurs in aqueous or atmospheric environments. The dissolution barrier of Mg atoms from the Mg matrix and the electrode potential can be significantly influenced by water. Sun et al.<sup>[24]</sup> proposed calculation methods of pure Mg with a single layer of water. Despite accounting for the role of water molecules, this model fails to adequately describe the solid–solution interface. Therefore, the development of a more realistic Mg/H<sub>2</sub>O model is essential to understand both the metal equilibrium potential and the dissolution kinetics of Mg atoms, ultimately advancing our understanding of the corrosion mechanisms and enhancing the corrosion resistance of Mg alloys.

In prior investigations on the metal/water interfaces, both explicit solvent model and implicit solvent model have been employed<sup>[25,26]</sup>; however, certain unresolved issues persist. Due to the inherent stochastic nature of H<sub>2</sub>O, achieving precise results in static conditions remains challenging. Ab initio molecular dynamics (AIMD) has become a prevalent tool for simulating the solvent effects of water, but time-consuming. AIMD simulations could average the impact of interfacial water configurations but also facilitate the exploration of structural properties, dynamics, rare events, and other pertinent factors.<sup>[27,28]</sup> For instance, Fogarty et al.<sup>[29]</sup> calculated the equilibrium potential of Mg(0001) to be  $-1.8$  V vs. SHE, which is somehow different from the result from the Nernst equation. On the other hand, umbrella sampling in conjunction with machine-learning potential had been employed to analyze the free energy barrier pertinent to solid phase transitions of GeSbTe.<sup>[30]</sup> Similar approaches could be applied to determine  $\Phi_e$ ,  $E_e$ , and  $\Delta G_{\text{Mg} \rightarrow \text{Mg}^{n+}}$  for Mg anodic corrosion reaction.

In this work, a relatively realistic model of the Mg/H<sub>2</sub>O interface has been established to investigate the corrosion

behavior of Mg alloy in water. Important parameters characterizing the corrosion rate,  $\Phi_e$ ,  $E_e$ , and  $\Delta G_{\text{Mg} \rightarrow \text{Mg}^{n+}}$ , have been obtained based on ab initio simulations for the anodic polarization curve of Mg in water. Additionally, we predict the impact of alloying elements on the corrosion behavior of Mg anodes. In sum, this study delves into the anodic dissolution kinetics of Mg alloys in water from the atomic scale, providing valuable insights for the development of corrosion-resistant Mg alloys.

## 2 | CALCULATION DETAILS

### 2.1 | Simulation models

Considering that (0001) surface is the most stable one for the HCP Mg,<sup>[23]</sup> a  $3 \times 2 \sqrt{3}$  Mg(0001) surface model with six atomic layers was constructed. Its surface energy and work function are determined to be 0.59 J/m<sup>2</sup> and 3.69 eV, respectively, which is consistent with prior works.<sup>[23,31]</sup> The bulk water box was created with the density of 1 g/cm<sup>3</sup>, where the  $a$  and  $b$  dimensions are same as those of Mg(0001) surface slab, while  $c$  dimensions are 20.38, 13.60, and 10.18 Å for 72, 48, and 36 water molecules, respectively. The Mg(0001)/ $n$  H<sub>2</sub>O interface models were constructed by combining Mg slab and bulk water box, as well as adding a vacuum region of 20, 20, and 16 Å for 72, 48, and 36 water molecules, respectively.

### 2.2 | Polarization curves

The equilibrium potential,  $E_e$ , can be calculated by the position difference between Fermi level of metals ( $E_{\text{fermi}}$ ) and the energy level for H<sub>2</sub>O/H<sub>2</sub> ( $E_{\text{H}_2\text{O}/\text{H}_2}$ ), as the following equation shows.

$$E_e = (E_{\text{H}_2\text{O}/\text{H}_2} - E_{\text{fermi}})/e \quad (3)$$

According to Trasatti's research study,<sup>[32]</sup> at ambient temperature, the energy level of H<sub>2</sub>O/H<sub>2</sub> is −4.44 eV with respect to the vacuum potential close to the surface of the solution ( $E_{\text{vac}}$ ). In this work, the vacuum potential outside the water and the position of  $E_{\text{H}_2\text{O}/\text{H}_2}$  in Mg(0001)/H<sub>2</sub>O model have been determined, as Figure 1c shows.  $E_{\text{fermi}}$  of Mg in Mg(0001)/H<sub>2</sub>O model can be obtained by electrostatic potential alignment between bulk Mg and bulk-like Mg in the interface model, as previously reported.<sup>[31]</sup>

Thus, the absolute electrode potential of Mg,  $\Phi_e$ , can be calculated as follows:

$$\Phi_e = E_e + 4.44. \quad (4)$$

$\Delta G_{\text{Mg} \rightarrow \text{Mg}^{n+}}$  can be depicted by the free energy barrier for one of Mg atoms in the Mg(0001) surface dissolved to water<sup>[33]</sup> by using constrained MD.

### 2.3 | Calculation methods

In this work, spin polarized calculations were performed using Vienna ab initio simulation package (VASP)<sup>[34]</sup> code with projector augmented wave<sup>[35]</sup> pseudopotentials to treat the ion–electron interactions. The wave functions were expanded in a plane-wave basis set with an energy cutoff of 520 eV. The generalized gradient approximation with the formula of Perdew–Burke–Ernzerhof<sup>[36]</sup> was used to calculate the exchange–correlation energies. Due to the high computational cost, only gamma point was used for all the calculations. DFT–D3 method<sup>[37,38]</sup> was used to correct van der Waals interaction. The convergence criteria for energy and force are set to  $1.0 \times 10^{-6}$  eV and 0.01 eV/Å, respectively.

In AIMD simulations, the optimized structures were heated to the target temperature of 300 K in 5 ps. For 36 H<sub>2</sub>O, 48 H<sub>2</sub>O, and 72 H<sub>2</sub>O interface models, the temperature of AIMD simulations (Figure S7) was maintained at 300 K with NVT ensemble (Nosé–Hoover thermostat) for 36, 40, and 18 ps with a time step of 1, 1, and 0.5 fs, respectively. The machine-learning force fields in VASP was used to accelerate the AIMD simulations, namely ML-AIMD. And the ML-AIMD simulations of 50 ps were performed for Mg/72 H<sub>2</sub>O interface model with the time step of 0.5 fs. The results without machine learning were used to verify the reliability of machine-learning force fields for the interface model.

Metadynamics<sup>[39]</sup> was used to simulate the potential energy surface (PES) for Mg atom dissolving from Mg (0001) surface with the Mg–Mg and Mg–O coordination numbers as CVs, enabling the estimation of the dissolution free-energy barrier of Mg atom. Gaussian hills with height 0.04 eV and width 0.08 eV were used.

## 3 | RESULTS AND DISCUSSION

### 3.1 | The effects of water thickness on the interaction of Mg–H<sub>2</sub>O

Firstly, the Mg/H<sub>2</sub>O interface structures with different water thickness, namely Mg(0001)/72 H<sub>2</sub>O, Mg(0001)/48 H<sub>2</sub>O and Mg(0001)/36 H<sub>2</sub>O, were analyzed. The number of water molecules adsorbed on the Mg surface within three models was demonstrated to be 3 or 4, corresponding to a coverage ratio of either 1/4 or 1/3 (Figure S1), which is consistent with the findings from prior investigations.<sup>[29]</sup> In Sun's research study,<sup>[24]</sup> they revealed that the quantities of water layers have limited influences on both the interface structure and charge transfer between water and Mg atoms by analyzing electron density redistribution of the Mg slabs covered with monolayer and bilayer water molecules. However, the difference of planer charge density difference between Mg (0001)/36 H<sub>2</sub>O and Mg(0001)/48 H<sub>2</sub>O model (see Figure S2) indicated that most water molecules interacted with Mg atoms in the Mg(0001)/36 H<sub>2</sub>O model, but in the Mg(0001)/

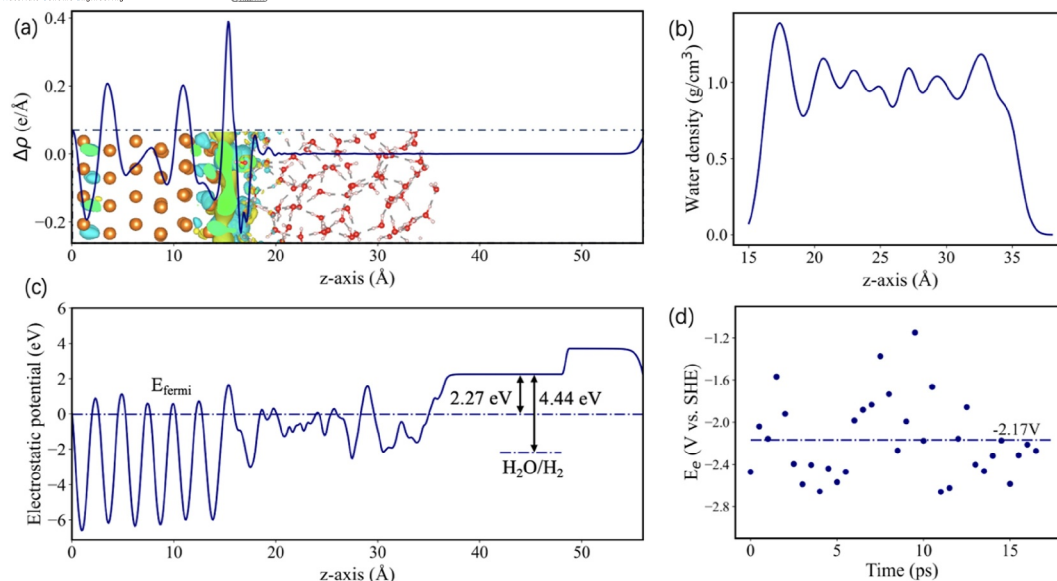


**FIGURE 1** (a) The planar charge density difference of Mg(0001)/72 H<sub>2</sub>O system in *z* direction ( $\Delta\rho = \rho_{\text{Mg}/72 \text{ H}_2\text{O}} - (\rho_{\text{Mg}} + \rho_{\text{H}_2\text{O}})$ ), where  $\rho_{\text{Mg}/72 \text{ H}_2\text{O}}$ ,  $\rho_{\text{Mg}}$ , and  $\rho_{\text{H}_2\text{O}}$  are the charge densities of the interface model, Mg(0001) slab and 72 H<sub>2</sub>O, respectively), (b) the water density distribution, and (c) the electrostatic potential of Mg(0001)/72 H<sub>2</sub>O along *z*-axis. (d) Equilibrium potential of Mg(0001)/72 H<sub>2</sub>O model during regular ab initio molecular dynamics simulation. The cell of interface model is schematically shown as the dashed rectangle in panel (a) and the dashed horizontal line in panel (d) represents the averaged  $E_e$  of  $-2.17$  V versus SHE. SHE, standard hydrogen electrode.

48 H<sub>2</sub>O model the outermost water molecules did not interact with Mg atoms. The average positions along *z*-axis of surface Mg atoms were also analyzed (Figure S3), which showed that the surface Mg atoms with H<sub>2</sub>O adsorption moved toward the water layer. The disparity in the average position along *z*-axis of surface Mg atoms, with and without the water molecule adsorption, was  $\sim 0.5$  Å in both the Mg(0001)/48 H<sub>2</sub>O and Mg(0001)/72 H<sub>2</sub>O model, whereas it was around 1.5 Å in the Mg(0001)/36 H<sub>2</sub>O model.

Considering water/vacuum interface and the electrical double layer (EDL) effect at the metal/water interface, it is necessary to include the water with adequate thickness to represent both the interfacial water and bulk water. Water molecules near interface have a tendency to align in the same direction, aggregate more closely and adsorb on Mg atoms, resulting in the higher interfacial water density.<sup>[40]</sup> Conversely, the density of bulk water is expected to be lower than the interface, approaching a value close to 1 g/cm<sup>3</sup>. Figure 1b shows that only the density of water layer at the Mg(0001)/72 H<sub>2</sub>O interface was larger than 1 g/cm<sup>3</sup>, the density of middle water layer was very similar to the bulk water, and overall average density of water is 1.00 g/cm<sup>3</sup>. Figure S4 shows the water density of Mg(0001)/36 H<sub>2</sub>O model and Mg(0001)/48 H<sub>2</sub>O model. Hence, the Mg(0001)/72 H<sub>2</sub>O model offers a more accurate representation of the interactions between metallic magnesium and aqueous solutions.

For 36 H<sub>2</sub>O, 48 H<sub>2</sub>O, and 72 H<sub>2</sub>O interface models, the snapshots were extracted at intervals of 1000 steps from the AIMD trajectories, the structures of which were further applied for the single point calculations to obtain the planar

averaged electrostatic potential for each snapshot interface model. Based on the above mentioned calculation methods,  $E_e$  and  $\Phi_e$  for every snapshot are calculated, respectively. The averaged  $E_e$  and  $\Phi_e$  over all the snapshots considered are  $-2.01$  (Figure S5) and  $2.43$  V for the Mg/36 H<sub>2</sub>O model, respectively,  $-1.85$  (Figure S5) and  $2.59$  V for the Mg/48 H<sub>2</sub>O model, respectively, and  $-2.17$  (Figure 1d) and  $2.27$  V for the Mg/72 H<sub>2</sub>O model, respectively. Fogarty et al.<sup>[29]</sup> reported that in the same water thickness as in the 48 H<sub>2</sub>O model, the  $\Phi_e$  value is 2.60 V, very close to our result of Mg(0001)/48 H<sub>2</sub>O, 2.59 V. The Mg(0001)/72 H<sub>2</sub>O model offers a more accurate representation of the interactions between metallic magnesium and aqueous solutions, and its  $E_e$  was closer to the experimental value of  $-2.37$  V.<sup>[32]</sup> Consequently, we employed it for further investigation of the corrosion behavior of magnesium.

To better understand the interactions between Mg and water molecules, AIMD simulation with machine-learning force fields was further performed for the Mg(0001)/72 H<sub>2</sub>O model for 50 ps, and the last 42 ps results from ML-AIMD simulations were used for further analysis. The number of adsorbed water molecules from ML-AIMD simulations is larger compared to that of standard AIMD. The accumulation of water molecules at the interface was evident, with a transition to bulk water behavior observed beyond 21 Å in *z*-axis (Figure 2a), and the overall average density was 0.92 g/cm<sup>3</sup>. Besides, the  $E_e$  and  $\Phi_e$  were calculated with the average values of  $-2.12$  and  $2.32$  V, respectively, which were very close to those calculated using standard AIMD. However, the simulation time cost is a few tenths of standard AIMD, and root mean square error of energy was around 0.0036 eV/



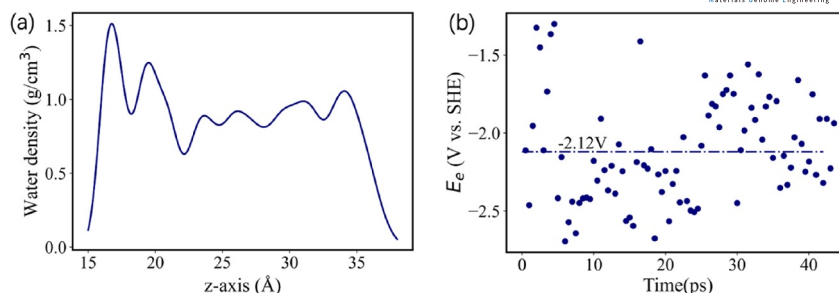


**FIGURE 2** (a) The water density distribution along z-axis and (b) equilibrium potential of Mg(0001)/72 H<sub>2</sub>O model during ML-ab initio molecular dynamics simulation (dashed line in panel (b) is the average equilibrium potential of −2.12 V).

atom. The results show that machining-learning force fields can greatly improve the rate of AIMD with the similar accuracy for properties of interests.

### 3.2 | The potential energy surface for Mg atom dissolution process

The free energy barrier ( $\Delta G_{\text{Mg} \rightarrow \text{Mg}^{n+}}$ ) of a Mg atom on the Mg(0001) surface dissolves to water was used to depict the activation energy for anodic dissolution process. Owing to the electrical neutrality of model, the electrical work of  $\text{Mg}^{n+}$  was not considered. Nevertheless, it is still possible to simulate the initial process of Mg dissolution. To obtain  $\Delta G_{\text{Mg} \rightarrow \text{Mg}^{n+}}$ , we used metadynamics to calculate the 2D-PES by using Mg-Mg and Mg-O coordination numbers as CVs. The bias potential (Gaussian hills) that acts on the CVs with a certain height and width is continuously added at certain intervals until there is enough simulation time to fulfill PES.<sup>[40]</sup> Previous studies rarely reported the direct determination of  $\Delta G_{\text{Mg} \rightarrow \text{Mg}^{n+}}$ . One reason is that enhanced sampling in AIMD simulations has high time-cost. Another reason is that the EDL is not easy to reasonably simulate.

During metadynamics simulation process, the complete Mg dissolution process encompasses: (i) Mg migration from the surface to transition state and an increase in coordination number of water and Mg from one to three; (ii) the coordination number of Mg and water from three to six, culminating in the formation of  $[\text{Mg}(\text{H}_2\text{O})_6]$  and the dissociation of a water molecule. The initial dissolution stages involve Mg leaving from the surface, increasing its water coordination number. This process aligned with the reaction pathway wherein Mg atoms interact with water molecules, forming  $\text{Mg} \cdot (\text{H}_2\text{O})_x$  complexes in aqueous electrolytes.<sup>[19]</sup> In this progress, Mg-Mg and Mg-O bonds are continuously formed or broken, at the same time, the bias potential was added continuously to fill the PES.

The calculated free energy surface, as depicted in Figure 3, exhibits two distinct local maximums representing the initial and final states of the Mg dissolution process. The activation energy barrier that the dissolution of 1 Mg atom

into water necessitates overcoming is determined to be 0.835 eV, compared with the 0.71 eV, accounts for 30% of the total energy needed to break chemical bonds to form ions and the surface energy density, reported in Ma's research study.<sup>[23]</sup> For future studies, we noticed that more advanced methods, such as well-tempered metadynamics,<sup>[41,42]</sup> could be applied to accelerate the sampling of the free energy potential surface.

### 3.3 | The anodic polarization curve

Based on the above calculated values, the anodic polarization curve for Mg can be readily constructed. The anodic exchange current density is  $1.14 \times 10^{-10}$  A/cm<sup>2</sup> using common transfer coefficient  $\alpha = 0.36$  and  $n = 1$  based on Equation (2).<sup>[23]</sup> Previous literature<sup>[43,44]</sup> has reported a solution with pH = 11 for the cathodic HER, featuring an cathodic exchange current density of  $10^{-8.1}$  A/cm<sup>2</sup> and an equilibrium cathodic electrode potential of  $E_e(\text{H}_2/\text{H}^+) = -0.63$  V vs. SHE using  $\alpha = 0.74$ ; the determined polarization curves of pure Mg are illustrated in Figure 4. During the electrochemical corrosion of pure Mg, cathodic and anodic reactions occur simultaneously at the same potential. When the corrosion current density reaches its peak value, the direction and rate of the anodic and cathodic reactions are opposite and equal.<sup>[43]</sup> These findings indicate that the corrosion current density attains its maximum value of  $10^{-5.26}$  A/cm<sup>2</sup> when the anodic and cathodic areas are proportioned at 36% and 64%, respectively. Concurrently, the corrosion potential is −1.33 V vs. SHE, indicated by the black star in Figure 4.

To validate the reliability of the calculation method, the calculated polarization curve was compared with the available experimental curves. As illustrated in Figure 4, the simulated polarization curves exhibit a good agreement with the experimental data. Several studies have elucidated that  $\text{Cl}^-$  ions can increase the corrosion current density and decrease the corrosion potential.<sup>[45,46]</sup> Consequently, the minor discrepancies, observed between calculated and experimental data depicted in Figure 4 may predominantly be attributed to the different concentration of  $\text{Cl}^-$  ions.

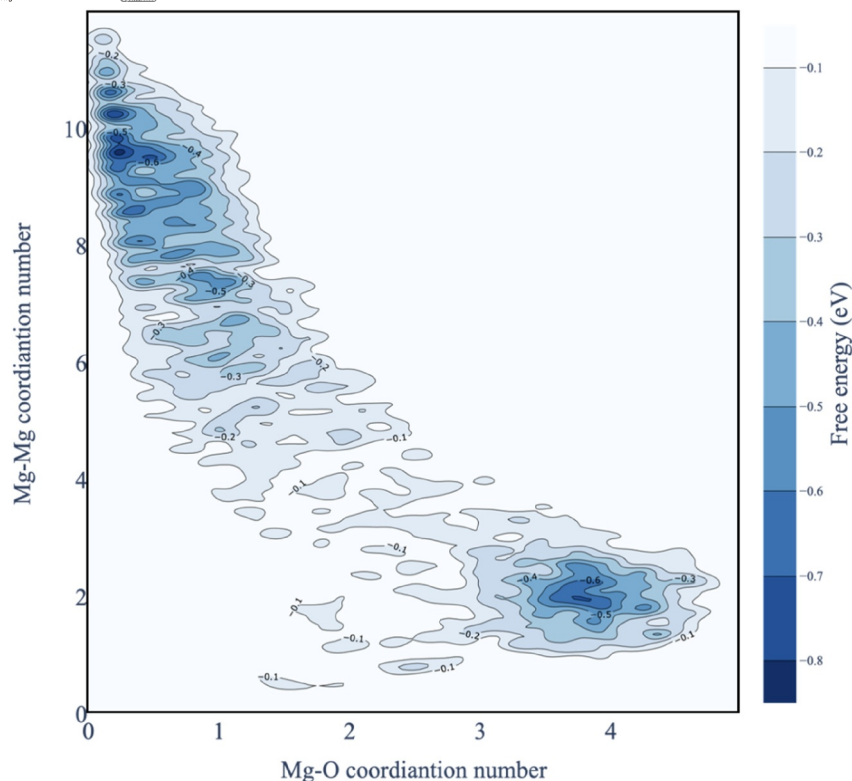


**FIGURE 3** The free energy landscape constructed from metadynamics simulation of Mg atom dissolution from Mg(0001) surface with the Mg-Mg and Mg-O coordination numbers as CVs at 300 K (with respect to the transition state energy).

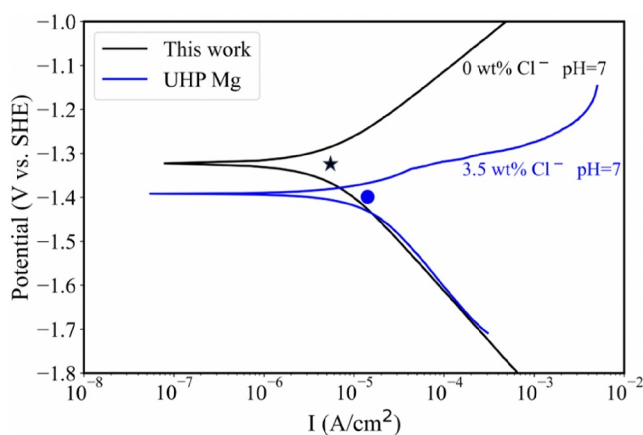


**FIGURE 4** The polarization curves of theoretical simulation and experimental data. UHP Mg was immersed in the 3.5 wt% NaCl solution with pH = 7 (see more details in Supporting Information S1). UHP, ultra-high-purity.

### 3.4 | Alloying effects on the anodic dissolution process

The effects of various alloying elements (Zn, La, Sc, Gd, Nd, Al, and Y) on anodic corrosion resistance of Mg were investigated from both thermodynamics and kinetics perspectives based on the alloyed Mg(0001)/72 H<sub>2</sub>O model. We

substituted one or 3 Mg atom (labeled as Mg<sub>71</sub>M and Mg<sub>69</sub>M<sub>3</sub>, respectively) within the second surface Mg layer with 7 possible alloying elements (Figure S6).

The  $E_e$  of Mg solid solution system was aligned with that of the Mg(0001)/72 H<sub>2</sub>O model based on work function of alloyed Mg slab. It is evident that alloying Zn, Al, and Mn into pure Mg significantly increase the  $E_e$  irrespective of the concentration as shown in Figure 5a. According to Equation (1), the more positive  $E_e$  is, the slower is the corrosion rate. Thus, these alloying elements can reduce the corrosion rate thermodynamically.

The free energy of Mg atoms with the dissolution process can be conceptualized into two parts: (i) overcome the interactions between the magnesium atom and its surrounding metallic atoms and become an isolated Mg atom and (ii) form a hexahydrate magnesium ion. It is posited that the contribution of the second part to the  $\Delta G_{\text{Mg} \rightarrow \text{Mg}^{n+}}$  remains similar in pure Mg and Mg alloy systems. In contrast, the contribution of the first component to the energy barrier can be interpreted as the formation energy of an Mg vacancy on Mg alloy surface. Then, the  $\Delta G_{\text{Mg} \rightarrow \text{Mg}^{n+}}$  were determined as the following equation:

$$E_V^{\text{alloy}} = E_V - E_{\text{perf}} + E_{\text{Mg}} \quad (5)$$

$$\Delta G_{\text{Mg} \rightarrow \text{Mg}^{n+}}^{\text{Alloy}} = E_V^{\text{alloy}} - E_V^{\text{Mg}} + \Delta G_{\text{Mg} \rightarrow \text{Mg}^{n+}} \quad (6)$$

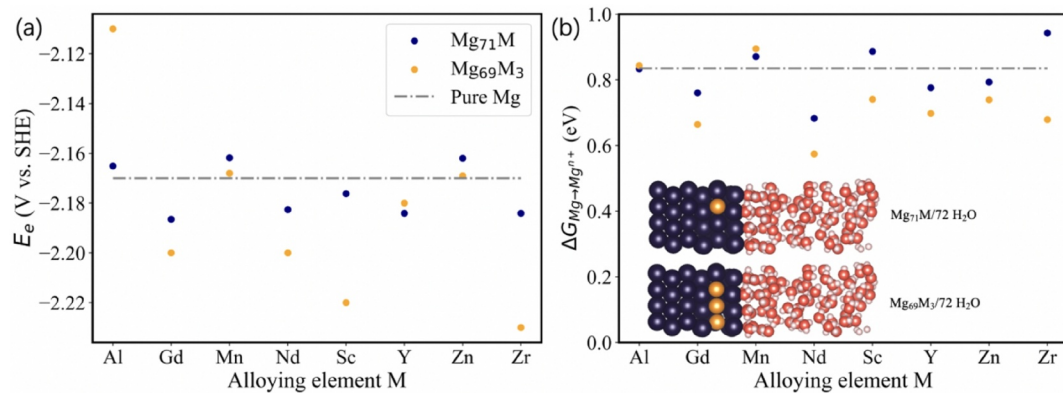


FIGURE 5 (a) The equilibrium potential  $E_e$  and (b) free energy barrier of Mg dissolution in Mg-alloying systems.

In Equation (5),  $E_V$  is the energy of the Mg-alloying slab with a vacancy on the surface;  $E_{\text{perf}}$  is the energy of the perfect Mg-alloying slab;  $E_{\text{Mg}}$  is the energy of an Mg atom. And  $E_V^{\text{alloy}}$  denotes the formation energy of surface Mg vacancy in the Mg-alloying slab. In Equation (6),  $E_V^{\text{Mg}}$  is the formation energy of surface Mg vacancy in the pure Mg slab. And  $\Delta G_{\text{Mg} \rightarrow \text{Mg}^{n+}}^{\text{Alloy}}$  denotes the predicted activation free energy of Mg dissolution in the Mg-alloying system. Figure 5b indicates that alloying with elements such as Al and Mn effectively elevate the activation energy of Mg dissolution, which inhibits the dissolution of Mg atoms kinetically.

According to our model with the same cathodic HER, good alloying elements shall show a lower corrosion current density and a higher corrosion potential. These two goals require to satisfy with both conditions of (i) a higher  $E_e$  than -2.17 V vs. SHE and (ii) a higher  $\Delta G_{\text{Mg} \rightarrow \text{Mg}^{n+}}$  than 0.835 eV. Alloying Al and Mn elements was expected to improve the corrosion resistance of Mg alloys. These results are consistent with prior experiments.<sup>[47,48]</sup> For Zn and Sc elements, although experimentally observed to reduce the corrosion rate, the reasons are mainly cathodic effect and more protective oxide film respectively, and the corrosion potential was lower than pure Mg, in agreement with our results.<sup>[49,50]</sup> For Nd, Gd, Y, and Zr elements, increased corrosion rate was observed experimentally.<sup>[51–53]</sup>

## 4 | CONCLUSION

In summary, this study has established a series of Mg(0001)/H<sub>2</sub>O models for the anodic corrosion of Mg, and the Mg(0001)/72 H<sub>2</sub>O model has been identified as the most optimal interface model. Through AIMD simulations, crucial parameters such as equilibrium potential and free energy barrier of Mg dissolution were computed, allowing for the theoretical derivation of anodic polarization curves that closely match experimental data. Additionally, our findings suggest that alloying with Al and Mn can enhance the corrosion resistance of Mg metal, as evidenced by calculated  $E_e$  and  $\Delta G_{\text{Mg} \rightarrow \text{Mg}^{n+}}$  for Mg-alloying systems. These insights pave the way for informed strategies in designing corrosion-resistant Mg alloys, underscoring the

importance of theoretical modeling and simulation techniques in corrosion research.

## AUTHOR CONTRIBUTIONS

**Jieqiong Yan:** Conceptualization; investigation; methodology; validation; software; formal analysis; data curation; writing—original draft; writing—review and editing. **Xinchen Xu:** Methodology. **Gaoning Shi:** Methodology. **Yao-wei Wang:** Software. **Chaohong Guan:** Software. **Yuyang Chen:** Methodology. **Yao Yang:** Writing—review and editing. **Tao Ying:** Writing—review and editing. **Hong Zhu:** Funding acquisition; writing—review and editing; visualization; resources; conceptualization; methodology; supervision. **Qingli Tang:** Methodology; conceptualization; writing—review and editing; writing—original draft; formal analysis; validation. **Xiaoqin Zeng:** Conceptualization; funding acquisition.

## ACKNOWLEDGMENTS

This work was financially supported by the National Key Research and Development Program of China (Nos. 2020YFB1505901, 2021YFB3501002), the National Natural Science Foundation of China (Grant No. 22106103, General Program No. 52072240), the Shanghai Science and Technology Committee (No. 18511109300), and the Science and Technology Commission of the CMC (2019JCQZD27300). First-principles calculations were carried out with computational resources from Shanghai Jiao Tong University Super Computer Center.

## CONFLICT OF INTEREST STATEMENT

The authors declare that they have no known competing financial interests or personal relationships that could have appeared to influence the work reported in this paper.

## DATA AVAILABILITY STATEMENT

The data that support the findings of this study are available from the corresponding author upon reasonable request.

## ORCID

Yao Yang <https://orcid.org/0000-0001-7483-927X>

Hong Zhu <https://orcid.org/0000-0001-7919-5661>

## REFERENCES

- Yan C, Xin Y, Chen XB, et al. Evading strength-corrosion tradeoff in Mg alloys via dense ultrafine twins. *Nat Commun.* 2021;12(1):4616.
- Xu W, Birbilis N, Sha G, et al. A high-specific-strength and corrosion-resistant magnesium alloy. *Nat Mater.* 2015;14(12):1229-1235.
- Liu BY, Liu F, Yang N, et al. Large plasticity in magnesium mediated by pyramidal dislocations. *Science.* 2019;365(6448):73-75.
- Han D, Zhang J, Huang J, Lian Y, He G. A review on ignition mechanisms and characteristics of magnesium alloys. *J Magnesium Alloys.* 2020;8(2):329-344.
- Atrons A, Shi Z, Mehreen SU, et al. Review of Mg alloy corrosion rates. *J Magnesium Alloys.* 2020;8(4):989-998.
- Wang Y, Xie T, Tang Q, et al. High-throughput calculations combining machine learning to investigate the corrosion properties of binary Mg alloys. *J Magnesium Alloys.* 2022;12(4):1406-1418.
- Prithivirajan S, Narendranath S, Desai V. Analysing the combined effect of crystallographic orientation and grain refinement on mechanical properties and corrosion behaviour of ECAPed ZE41 Mg alloy. *J Magnesium Alloys.* 2020;8(4):1128-1143.
- Atrons A, Song GL, Cao F, Shi Z, Bowen PK. Advances in Mg corrosion and research suggestions. *J Magnesium Alloys.* 2013;1(3):177-200.
- Taltavull C, Torres B, Lopez AJ, et al. Corrosion behaviour of laser surface melted magnesium alloy AZ91D. *Mater Des.* 2014;57:40-50.
- Abbas G, Liu Z, Skeldon P. Corrosion behaviour of laser-melted magnesium alloys. *Appl Surf Sci.* 2005;247(1-4):347-353.
- Córdoba LC, Montemor MF, Coradin T. Silane/TiO<sub>2</sub> coating to control the corrosion rate of magnesium alloys in simulated body fluid. *Corrosion Sci.* 2016;104:152-161.
- Ivanou DK, Starykevich M, Lisenkov AD, et al. Plasma anodized ZE41 magnesium alloy sealed with hybrid epoxy-silane coating. *Corrosion Sci.* 2013;73:300-308.
- Li J, Bai H, Feng Z. Advances in the modification of silane-based sol-gel coating to improve the corrosion resistance of magnesium alloys. *Molecules.* 2023;28(6):2563.
- Ren C, Ma L, Zhang D, Li X, Mol A. High-throughput experimental techniques for corrosion research: a review. *Mater Genome Eng Adv.* 2023;1(2):e20.
- Cao F, Shi Z, Hofstetter J, et al. Corrosion of ultra-high-purity Mg in 3.5% NaCl solution saturated with Mg(OH)<sub>2</sub>. *Corrosion Sci.* 2013;75:78-99.
- Zhu Q, Li Y, Cao F, et al. Towards development of a high-strength stainless Mg alloy with Al-assisted growth of passive film. *Nat Commun.* 2022;13(1):5838.
- Thomas S, Medhekar NV, Frankel GS, Birbilis N. Corrosion mechanism and hydrogen evolution on Mg. *Curr Opin Solid State Mater Sci.* 2015;19(2):85-94.
- Song GL, Shi Z. Corrosion mechanism and evaluation of anodized magnesium alloys. *Corrosion Sci.* 2014;85:126-140.
- Yuwono JA, Birbilis N, Taylor CD, Williams KS, Samin AJ, Medhekar NV. Aqueous electrochemistry of the magnesium surface: thermodynamic and kinetic profiles. *Corrosion Sci.* 2019;147:53-68.
- Williams KS, Rodriguez-Santiago V, Andzelm JW. Modeling reaction pathways for hydrogen evolution and water dissociation on magnesium. *Electrochimica Acta.* 2016;210:261-270.
- Yang Z, Wang J, Zhang C, et al. First-principle screening of corrosion resistant solutes (Al, Zn, Y, Ce, and Mn) in Mg alloys for Integrated Computational Materials Engineering guided stainless Mg design. *Mater Genome Eng Adv.* 2024;2(1):e22.
- Bockris JO, Mannan RJ, Damjanovic A. Dependence of the rate of electrochemical redox reactions on the substrate. *J Chem Phys.* 1968;48(5):1898-1904.
- Ma H, Chen XQ, Li R, Wang S, Dong J, Ke W. First-principles modeling of anisotropic anodic dissolution of metals and alloys in corrosive environments. *Acta Mater.* 2017;130:137-146.
- Sun H, Su G, Zhang Y, et al. First-principles modeling of the anodic and cathodic polarization to predict the corrosion behavior of Mg and its alloys. *Acta Mater.* 2023;244:118562.
- Taylor CD. Atomistic modeling of corrosion events at the interface between a metal and its environment. *Int J Corros.* 2012;2012:1-13.
- Bramley G, Nguyen MT, Glezakou VA, Rousseau R, Skylaris CK. Reconciling work functions and adsorption enthalpies for implicit solvent models: a Pt (111)/water interface case study. *J Chem Theor Comput.* 2020;16(4):2703-2715.
- Wang J, Román-Pérez G, Soler JM, Artacho E, Fernández-Serra MV. Density, structure, and dynamics of water: The effect of van der Waals interactions. *J Chem Phys.* 2011;134(2):024516.
- Ruiz Pestana L, Marsalek O, Markland TE, Head-Gordon T. The quest for accurate liquid water properties from first principles. *J Phys Chem Lett.* 2018;9(17):5009-5016.
- Fogarty RM, Li BX, Harrison NM, Horsfield AP. Structure and interactions at the Mg(0001)/water interface: an *ab initio* study. *J Chem Phys.* 2022;156(24):244702.
- Zhao Y, Sun J, Yang L, Zhai D, Sun L, Deng W. Umbrella sampling with machine learning potentials applied for solid phase transition of GeSbTe. *Chem Phys Lett.* 2022;803:139813.
- Luo Z, Zhu H, Ying T, Zeng X. First principles calculations on the influence of solute elements and chlorine adsorption on the anodic corrosion behavior of Mg (0001) surface. *Surf Sci.* 2018;672:68-74.
- Trasatti S. The absolute electrode potential: an explanatory note: (recommendations 1986). *Pure Appl Chem.* 1986;58(7):955-966.
- Réocreux R, Girel É, Clabaut P, et al. Reactivity of shape-controlled crystals and metadynamics simulations locate the weak spots of alumina in water. *Nat Commun.* 2019;10(1):3139.
- Kresse G, Furthmüller J. Efficiency of *ab-initio* total energy calculations for metals and semiconductors using a plane-wave basis set. *Comput Mater Sci.* 1996;6(1):15-50.
- Kresse G, Furthmüller J. Efficient iterative schemes for *ab initio* total-energy calculations using a plane-wave basis set. *Phys Rev B.* 1996;54(16):11169-11186.
- Perdew JP, Burke K, Ernzerhof M. Generalized gradient approximation made simple. *Phys Rev Lett.* 1996;77(18):3865-3868.
- Grimme S, Antony J, Ehrlich S, Krieg H. A consistent and accurate *ab initio* parametrization of density functional dispersion correction (DFT-D) for the 94 elements H-Pu. *J Chem Phys.* 2010;132(15):154104.
- Grimme S, Ehrlich S, Goerigk L. Effect of the damping function in dispersion corrected density functional theory. *J Comput Chem.* 2011;32(7):1456-1465.
- Laio A, Parrinello M. Escaping free-energy minima. *Proc Natl Acad Sci USA.* 2002;99(20):12562-12566.
- Li P, Huang J, Hu Y, Chen S. Establishment of the potential of zero charge of metals in aqueous solutions: different faces of water revealed by *ab initio* molecular dynamics simulations. *J Phys Chem C.* 2021;125(7):3972-3979.
- Barducci A, Bussi G, Parrinello M. Well-tempered metadynamics: a smoothly converging and tunable free-energy method. *Phys Rev Lett.* 2008;100(2):020603.
- Biswas S, Yamijala SS, Wong BM. Degradation of per- and poly-fluoroalkyl substances with hydrated electrons: a new mechanism from first-principles calculations. *Environ Sci Technol.* 2022;56(12):8167-8175.
- Luo Z, Xu J, Wang Y, et al. Theoretical analysis of the galvanic corrosion behavior of Mg-Ge binary alloy. *J Electrochem Soc.* 2019;166(13):C421-C427.
- Ma H, Wu L, Liu C, et al. First-principles modeling of the hydrogen evolution reaction and its application in electrochemical corrosion of Mg. *Acta Mater.* 2020;183:377-389.
- Ambat R, Aung NN, Zhou W. Studies on the influence of chloride ion and pH on the corrosion and electrochemical behaviour of AZ91D magnesium alloy. *J Appl Electrochem.* 2000;30:865-878.



46. Zhao MC, Liu M, Song GL, Atrens A. Influence of pH and chloride ion concentration on the corrosion of Mg alloy ZE41. *Corrosion Sci.* 2008;50(11):3168-3178.
47. Yang L, He S, Yang C, et al. Mechanism of Mn on inhibiting Fe-caused magnesium corrosion. *J Magnesium Alloys.* 2021;9(2):676-685.
48. Pardo A, Merino MC, Coy AE, Arrabal R, Viejo F, Matykina E. Corrosion behaviour of magnesium/aluminium alloys in 3.5wt.% NaCl. *Corrosion Sci.* 2008;50(3):823-834.
49. Zhang C, Wu L, Liu H, et al. Microstructure and corrosion behavior of Mg-Sc binary alloys in 3.5 wt.% NaCl solution. *Corrosion Sci.* 2020;174:108831.
50. Kubásek J, Vojtěch D. Structural characteristics and corrosion behavior of biodegradable Mg-Zn, Mg-Zn-Gd alloys. *J Mater Sci Mater Med.* 2013;24(7):1615-1626.
51. Liu M, Schmutz P, Uggowitzer PJ, Song G, Atrens A. The influence of yttrium (Y) on the corrosion of Mg-Y binary alloys. *Corrosion Sci.* 2010;52(11):3687-3701.
52. Zhao X, Shi L, Xu J. A comparison of corrosion behavior in saline environment: rare Earth metals (Y, Nd, Gd, Dy) for alloying of biodegradable magnesium alloys. *J Mater Sci Technol.* 2013;29(9):781-787.
53. Gandel DS, Easton MA, Gibson MA, Abbott T, Birbilis N. The influence of zirconium additions on the corrosion of magnesium. *Corrosion Sci.* 2014;81:27-35.

## SUPPORTING INFORMATION

Additional supporting information can be found online in the Supporting Information section at the end of this article.

**How to cite this article:** Yan J, Xu X, Shi G, et al. The anodic dissolution kinetics of Mg alloys in water based on ab initio molecular dynamics simulations. *MGE Advances.* 2024;e47. <https://doi.org/10.1002/mgea.47>